(Received 25 October 2025, Accepted 24 November 2025, Scheduled 23 December 2025)

Design of Wideband Cycle-Shaped Multi Resonant Antenna for Sub 6-GHz, WLAN, ISM, Applications

Chennoju Jaya Prakash[1], Vasudha Vijayasri Bolisetty[2], Bhupathi Ajay Kumar[3], Udara Yedukondalu[4], and Bokkisam Venkata Sai Sailaja[5, *]

[1]*Department of Electronics and Communication Engineering, Sir C R Reddy College of Engineering Eluru, Andhra Pradesh 534007, India*
[2]*Department of ECE, Aditya University, Surampalem 533437, India*
[3]*Department of Electronics and Communication Engineering, SR Gudlavalleru Engineering College Vijayawada, Andhra Pradesh 521356, India*
[4]*Department of ECE, MVR College of Engineering and Technology, Paritala-521180, Andhra Pradesh, India*
[5]*Department of Electronics and Communication Engineering, Koneru Lakshmaiah Education Foundation Vaddeswaram, Guntur-522502, India*

ABSTRACT: This work introduces a small cycle-shaped antenna for multiband applications. The design combines three main ideas, concentric circular rings on the patch, spoke-like arms to excite higher frequencies, and a hexagonal slot in the ground to extend bandwidth. The antenna is built on a $40 \times 42 \times 1.6\,\text{mm}^3$ FR-4 substrate and works across three frequency bands within 3.04–3.62 GHz and 5.07–8.08 GHz, suitable for sub-6 GHz, ISM, WLAN applications. The structure is easy to tune, and increasing rings and the length of the spokes shifts the resonance to lower frequencies. Smaller gaps between rings may increase coupling and bandwidth. A bigger hexagonal slot etched on the ground widens the range but may slightly shift the frequency. With these features, the antenna achieves strong resonances and good return loss at 3.31, 5.75, and 7.58 GHz, achieving S_{11} of -19.4 dB, -34.9 dB, -21.4 dB showing that it can support wireless applications.

1. INTRODUCTION

Wireless communication has been developed very rapidly over the past few decades, during which it caught everyone's attention. Today, all these devices need to support Wi-Fi, WLAN, and also WiMAX without increasing their cost and size [1]. Smaller antenna structures are becoming popular due to their smaller dimensions. Engineers are mostly focusing on designs that can achieve more with less space (multiband, wideband, and efficient) [2]. Due to this need, engineers have explored various antenna structures such as adding slots, integrating ring structures, adding additional slits, and etching slots on the ground plane to improve performance [3–5]. In [6], a 3D antenna operating from 1.10 to 2.20 GHz has a complex structure and fails to produce high gain. In [7], a Vivaldi antenna with an impedance bandwidth of 0.55 GHz is reported, but it cannot provide sufficient bandwidth or isolation. A unique dual-band slot antenna is presented in [8], where arc-shaped slots are inserted into two semicircular slots on the ground to achieve the desired frequencies. In [19], a triangular slotted antenna is transformed into a floral-shaped slot. In [9], an antenna for sub-6 GHz applications is discussed; however, its physical size is relatively large.

In [10], the importance of slits and slots on improving impedance matching is discussed. Engineers have developed many circularly polarized symmetric slotted antennas. Among them, cross-shaped polarized symmetric slot antennas perform better than many other shapes, as reported in [11]. In [12], another compact single-feed circularly polarized antenna is introduced with diagonal slits on the patch. In [13], an asymmetric circular patch antenna for Radio Frequency Identification (RFID) applications is presented. Increasing effective substrate thickness can improve the bandwidth, and integrating an inverted-U shaped structure increases the electrical length of the design, as discussed in [14]. Several antenna structures have been introduced to generate circular polarization. Examples include circular slots with split-ring resonators [18], asymmetric structures [16], uneven C-shaped slots [15], V-shaped slits [20], and cross-slot coupling techniques [17], all reported in the literature.

A circular patch antenna with a pentagon slot is presented in [21]. To achieve better performance, different slot techniques are discussed in [22]. A meander-line antenna array for multiple-input multiple-output (MIMO) applications is reported in [23]. Many of these applications are battery-powered handheld devices; regular charging ensures smooth communication [28]. Energy harvesting from surrounding radio frequency (RF) signals can support wireless systems [24]. Microstrip patch antennas and wideband antennas with metamaterials are considered for RF energy harvesting in [25–27, 29]. Circular and ring-shaped antennas are often preferred because they operate at multiple frequencies without increasing size.

* Corresponding author: Bokkisam Venkata Sai Sailaja (sailajabokkisam@gmail.com).

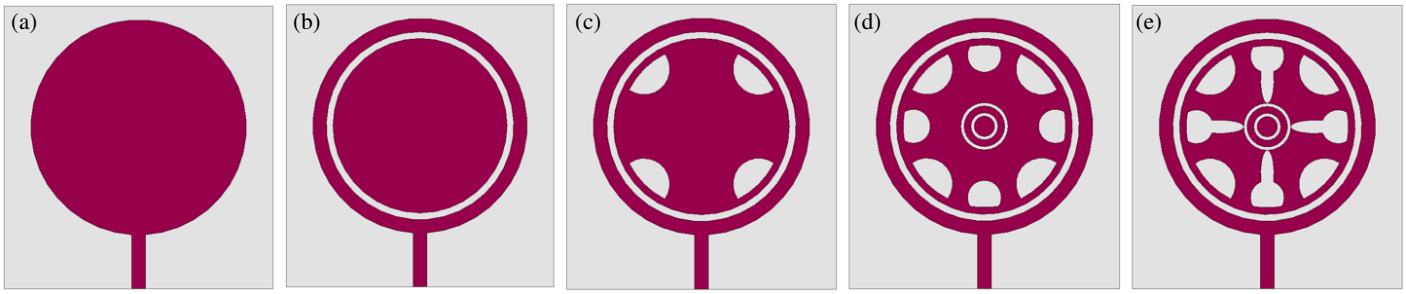

FIGURE 1. The evolution of the CCRA design followed a four-step process, initiating from the Ant 1 and resulting in the final configuration at Ant 5.

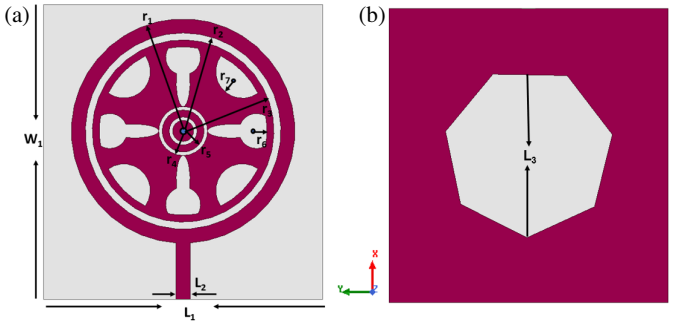

FIGURE 2. Configuration of cycle-shaped circular ring antenna with (a) top and (b) bottom view.

To reduce the interference from WLAN, WiMAX, and satellite services, the authors in [30] suggest a small ultra-wideband (UWB) MIMO monopole antenna with three integrated notch bands. A small multiband monopole MIMO antenna that can function in the 2.4, 3.5, and 5–6 GHz wireless bands is presented in [31]. To improve directivity, a superdirective wideband array that uses circular monopole components loaded with parasitic patches is presented in [32]. Still, some of the studies from the literature show strong performance [30–32].

The antenna presented in this work is developed using a compact cycle-shaped circular ring antenna (CCRA) structure combined with semicircular slots to achieve multiband performance. To further optimize performance, the ground plane is etched with a hexagon slot, which strengthens impedance matching and supports stable resonances. The rings and spokes that determine the antenna performance-larger dimensions shift the resonance to lower frequencies, while smaller geometry moves the frequency upward. The bandwidth is controlled by the ring spacing and hexagon slot size; smaller gaps or larger slots result in wider bandwidth. Placing the feed near strong current points improves impedance matching and performance. The proposed CCRA design is analysed using electromagnetic simulation tools. Radiation patterns and gain metrics are obtained through ANSYS High Frequency Structure Simulator (HFSS).

2. ANTENNA DESIGN

A single circular annular ring with cycle-shaped slots is operated at several bands. The antenna is smaller in its overall dimension, and it is approximately $40 \times 42 \times 1.6\,\text{mm}^3$, fabricated on FR-4 with a thickness of 1.6 mm. Moreover, the ground plane of the design is etched with a hexagon shape for better enhancement. In the device testing phase, they both resonate greatly with good reflection coefficients. The measured reflection coefficient values show that the antenna resonates well at the respective resonances. The design is constructed incrementally (as specified in Figure 1), ranging from a simple circular ring patch to arranging ring slots until they obtained the final required band. The evolution of the CCRA design followed a four-step process, initiating from Ant 1 and resulting in the final configuration at Ant 5, as shown in Figure 1. The final configuration of the CCRA antenna design is shown in Figure 2. Key parameters of the CCR antenna geometry are provided in Table 1.

These rings look like the spokes of a bicycle wheel, hence their circular nature. The electrical length is increased, and multiple correlated current paths are formed due to the presence of several rings, which contribute to achieving multi-resonant modes and broadening bandwidth. Then, spoke-like features (or tear-dropped arms) appear from the outer ring toward the centre. The spokes are typically arranged in four particularly consecutive, but also non-consecutive pairs. A hexagon slot is etched at the centre of the ground plane of the antenna.

The proposed CCRA design achieves multiband behaviour at each step in the design and introduces new resonating lengths and paths. In Figure 1(a) Ant 1, the plain circular patch operates at a single frequency band. In Figure 1(b), a circular ring is etched, forming an additional ring loop for surface currents, displaying a shallow dip indicating weak resonance. In Figure 1(c), four semicircular slots disturb the current flow and add another strong resonance with a deep notch and better coupling. In Figure 1(d) and Figure 1(e), additional inner rings and spoke-shaped slots are integrated, which further increase the effective current length and lead to new frequency bands. As the design is developed by adding circular rings, polygon slots, and the modified ground, new resonances appear.

The fabrication model of the CCR antenna with connectors is shown in Figure 3. The notches in the curves represent the frequencies where impedance matching occurs. Finally, in Figure 4, the measured S_{11} values are compared with the final configuration antenna in Figure 5. The simulated curve is represented in black, and the measured curve is represented in red. Their values closely match and prove that the fabricated design operates the same as the simulated design. Eventually, Fig-

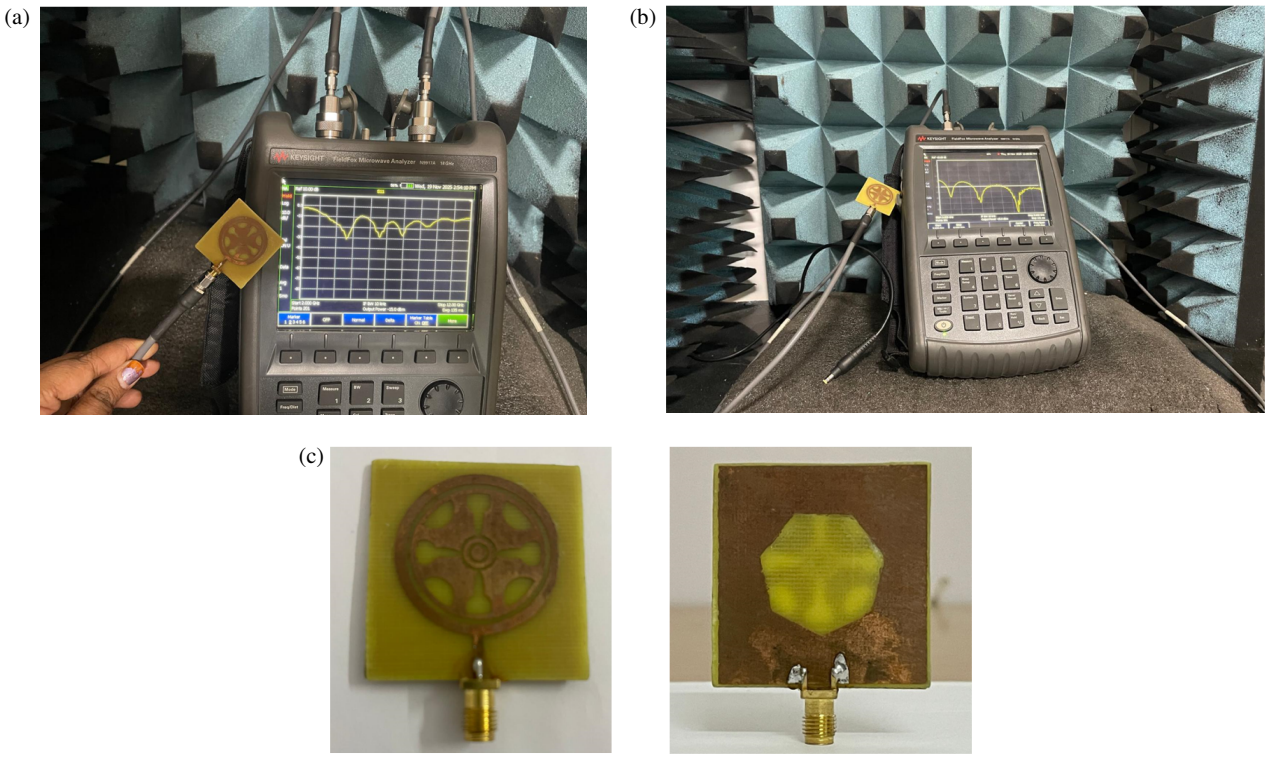

FIGURE 3. (a) CCRA connected to network analyser measured S_{11}. (b) Axial ratio. (c) Fabricated design with connector.

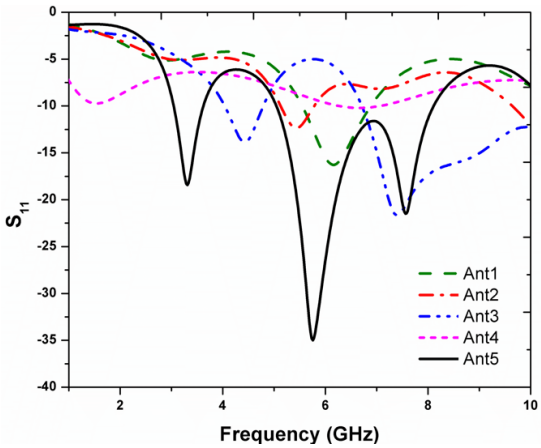

FIGURE 4. Step wise comparison of the antenna design results comparison highlighting to final improvement.

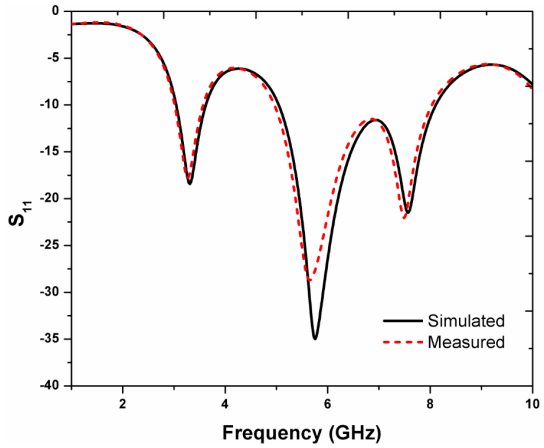

FIGURE 5. Comparative results of simulated and measured based on S_{11} consistency across operating band.

TABLE 1. Key parameters of the CCRA geometry.

Dimension	Value (mm)	Dimension	Value (mm)
L_1	40	r_3	13
W_1	42	r_4	3.5
L_2	2	r_5	3
L_3	12	r_6	2.5
r_1	16	r_7	1.9
r_2	14	a	3.5

ure 6 exhibits the voltage standing wave ratio (VSWR) results for measured and simulated cases.

These equations explain how the effective radius is determined by taking into account the ring-shaped geometry. With these parameters, the resonant frequency of the antenna is finally obtained through the expressions given in Equations (1)–(7). The specifications of the circular ring-slotted antenna are shown in Table 1. Here, the resonant frequency is calculated by three techniques.

Half wave microstrip slot model ($\lambda/2$)

$$f_{res} = \frac{c}{2L\sqrt{\varepsilon_{eff}}}, \quad L = \frac{c}{2f_{res}\sqrt{\varepsilon_{eff}}} \tag{1}$$

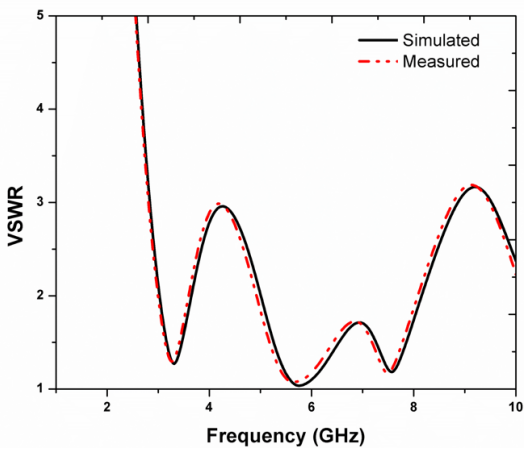

FIGURE 6. Measured VSWR performance of the antenna.

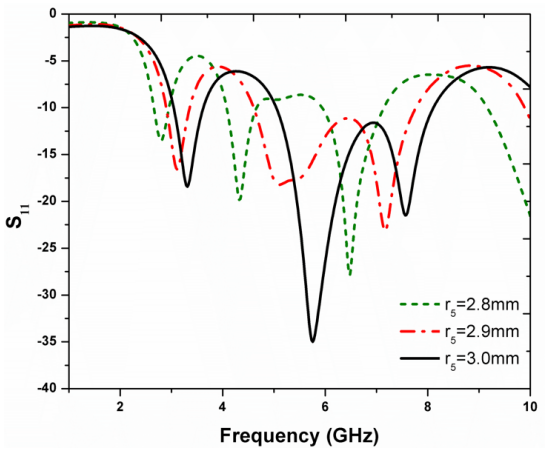

FIGURE 7. S_{11} characteristics for different configurations of r_5.

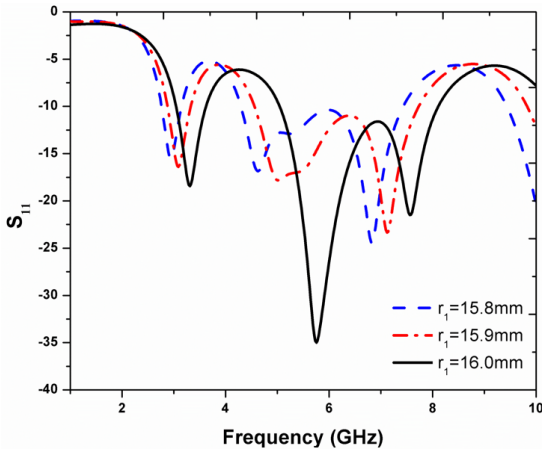

FIGURE 8. S_{11} characteristics for different configurations of r_1.

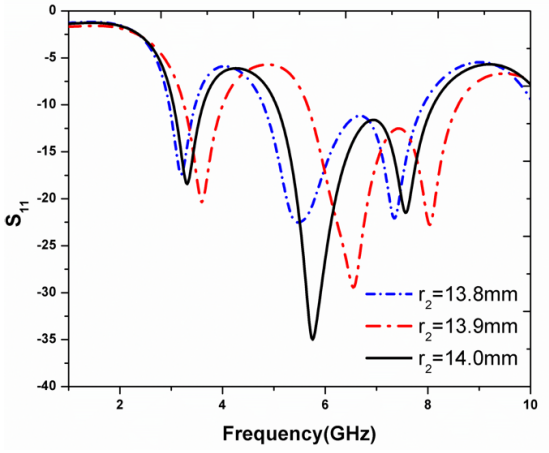

FIGURE 9. S_{11} characteristics for different configurations of r_2.

Circular patch TM_{11} is approximated by

$$f_{res} = \frac{X_{11}c}{2\pi a\sqrt{\varepsilon_r}}, \quad a = \frac{X_{11}c}{2\pi f_{res}\sqrt{\varepsilon_r}} \tag{2}$$

Ring slot circumference model, when mean circumference ≈ guided wavelength

$$2\pi r_{eff} \approx \lambda_g, \quad f_{res} = \frac{c}{2\pi r_{eff}\sqrt{\varepsilon_{eff}}} \tag{3}$$

$$r_{eff} = \frac{c}{2\pi f_{res}\sqrt{\varepsilon_{eff}}} \tag{4}$$

Guided wavelength

$$\lambda_g = \frac{c}{f_{res}\sqrt{\varepsilon_{eff}}} \tag{5}$$

Patch radius is used to reduce resonance

$$F = \frac{8.791 \times 10^9}{f_{res}\sqrt{\varepsilon_r}} \tag{6}$$

$$a = \frac{F}{\sqrt{1 + \frac{2h}{\pi\varepsilon_r F}\left[\ln\left(\frac{\pi F}{2h}\right) + 1.7726\right]}} \tag{7}$$

F = scaling factor and f_{res} = actual frequency.

3. RESULTS AND DISCUSSION

The simulated S_{11} characteristics of the CCR antenna for different values of dimensions r_1, r_2, r_3, and r_4 are analyzed. All these parameters r_1, r_2, r_3, r_4, and r_6 are varied to notice their impact on the impedance matching and operating frequency features over the frequency range of 1–10 GHz. It can be analysed that minor changes within these radii majorly affect both the resonant band shift and the drop in the return loss. As r_1 (Figure 8) varies from 15.8 mm to 16.0 mm, the lower band shifts toward higher operating frequencies, demonstrating responsiveness in the antenna's electrical length. In the same manner, increasing r_2 (Figure 9) changes the coupling within the radiating patch and produces good changes in bandwidth and operating frequency stability. The parameter r_3 (Figure 10) impacts the tuning of the network and impedance matching when $r_6 = 2.5$ mm, resulting in an S_{11} below -35 dB at nearly 6 GHz. This shows that r_6 plays a major role in vary-

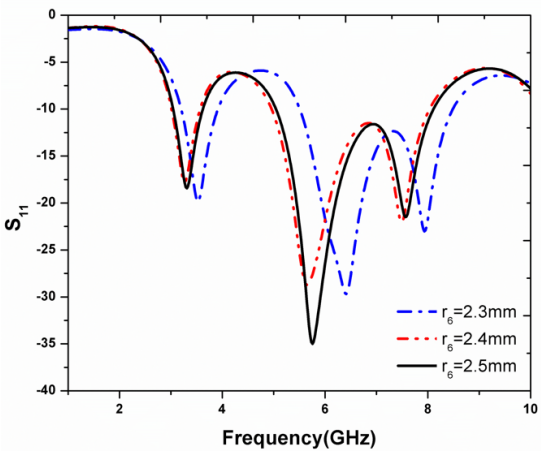

FIGURE 10. S_{11} characteristics for different configurations of r_6.

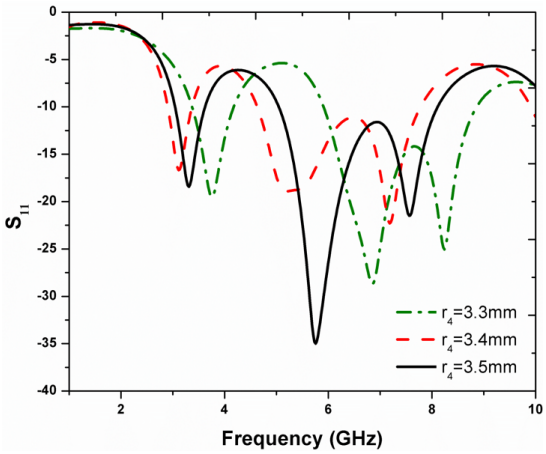

FIGURE 11. S_{11} characteristics for different configurations of r_4.

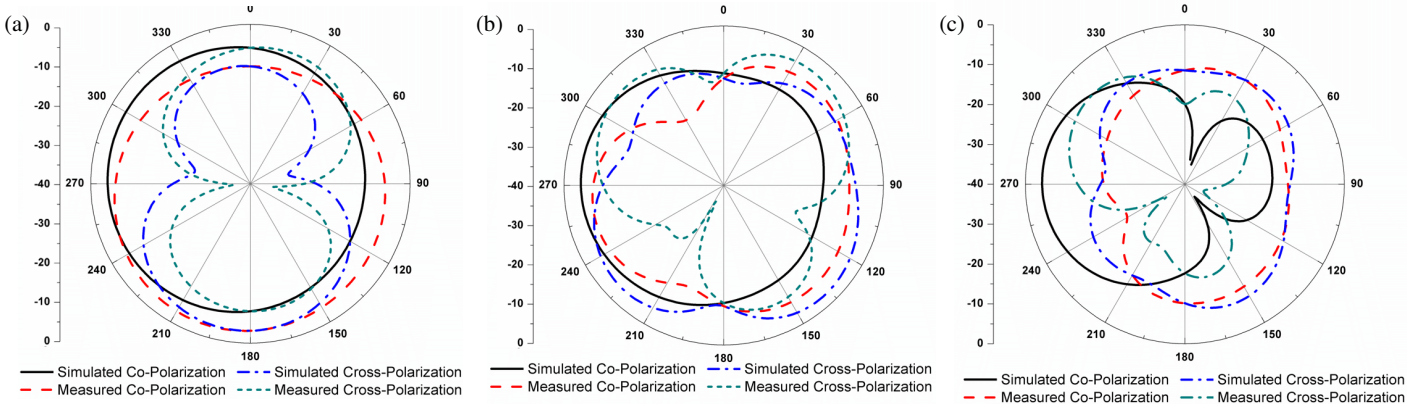

FIGURE 12. Analysing co-pol and x-pol at (a) 3.31 GHz, (b) 5.75 GHz, (c) 7.58 GHz.

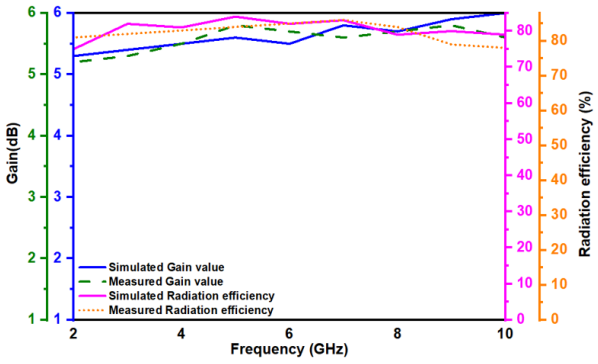

FIGURE 13. Variation of gain and RE across frequency minimal showing the consistent gain characteristics.

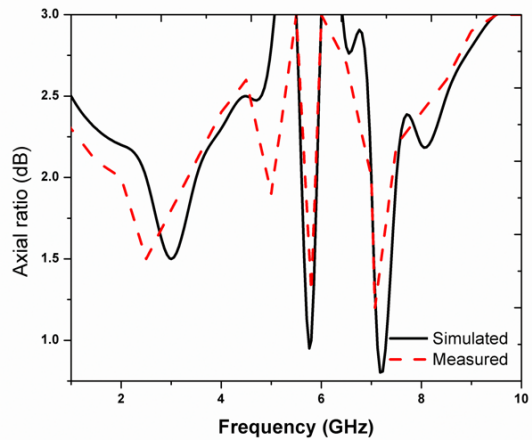

FIGURE 14. Axial ratio of the design showing losses over the operating frequency.

ing the return loss and resonance peak. Similarly, differences in r_4 (Figure 11) mostly influence the resonance frequency and bandwidth. When r_4 is tuned to 3.5 mm, the design demonstrates good reflection performance. The parameter r_5 (Figure 7) impacts the tuning of the network and impedance matching when $r_5 = 2.8$ mm, resulting in an S_{11} below -30 dB at nearly 6 GHz. This shows that r_5 plays a major role in varying the return loss and resonance peak. Similarly, differences in r_4 mostly influence the resonance frequency and bandwidth. When r_4 is tuned to 3.5 mm, the design demonstrates good reflection performance, exhibiting improved characteristics. To sum up, the parametric analysis shows that all the radii contribute to the electromagnetic response.

The proposed simulated and measured co-pol and x-pol at 3.31 GHz, 5.75 GHz, and 7.31 GHz are shown in Figure 12. The plots of both the co-polarization and cross-polarization configurations are seen in Figure 12. At the 3.31 GHz fre-

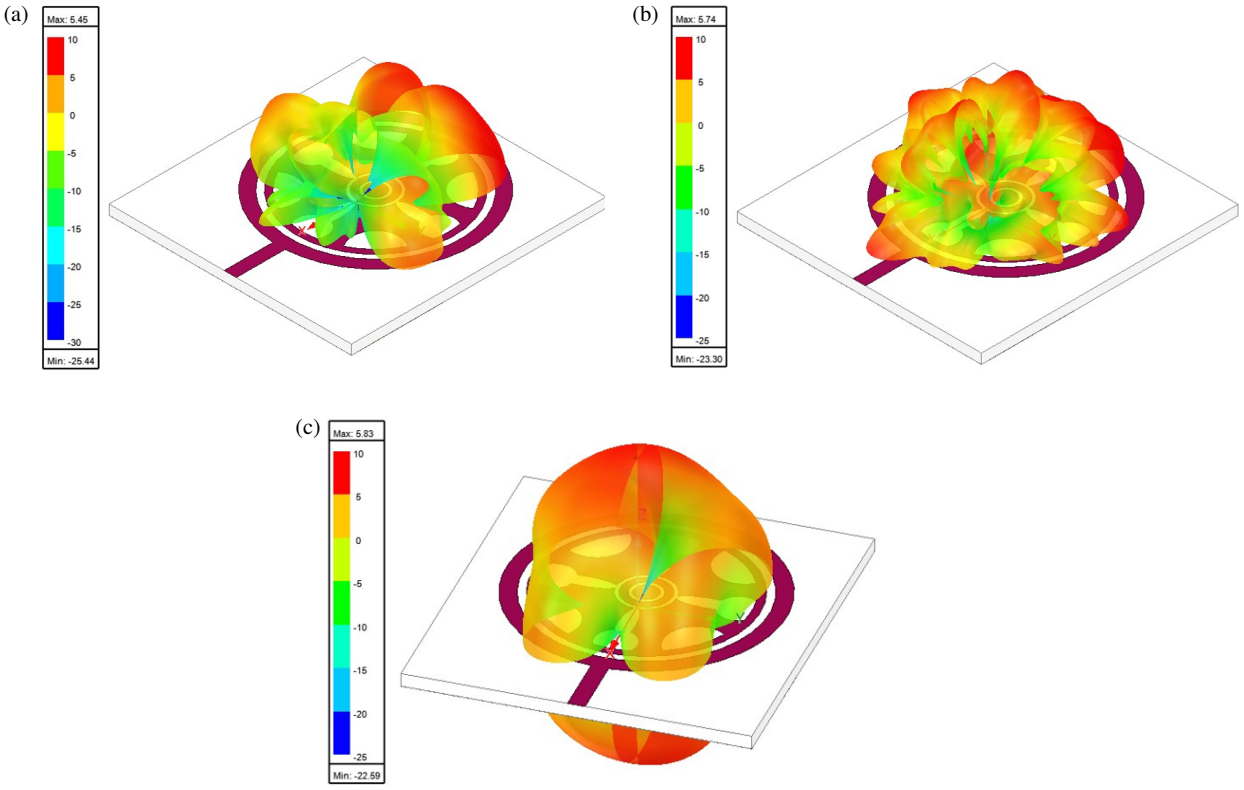

FIGURE 15. 3D radiation characteristic, with the schematic of the patch antenna (a) 3.31 GHz, (b) 5.75 GHz, (c) 7.58 GHz.

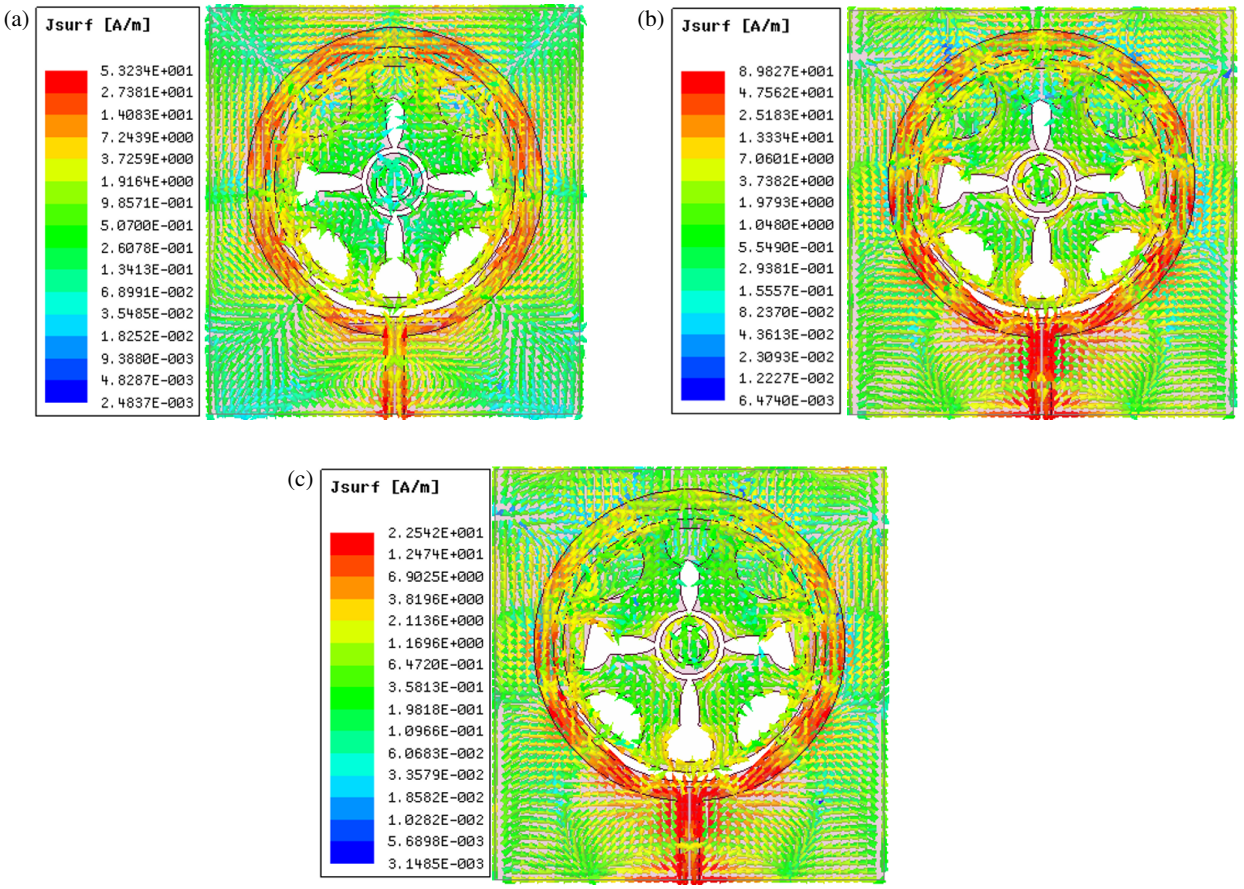

FIGURE 16. Demonstrating variation of current flows at different three operating frequencies at different angles.

TABLE 2. Performance comparison of the CCRA design with other designs available in literature.

Reference	Antenna Size (λ_0)	Operating Bands (GHz)	Achieved Bandwidth (GHz)	S_{11} (dB)	Peak Gain (dBi)
[29]	0.308×0.185	1.85 3.3	1.75–1.95 3.2–3.4	-14 -13	2.88 5.8
[24]	0.245×0.490	2.45 5.8	2.3–2.55 5.65–5.92	-25 -19	4.8 6
[27]	0.440×0.463	3.47 6.96	3.3–3.6 6.7–7.4	-25.8 -28.4	4.3 5.8
[25]	0.317×0.208	2.5	2.4–6.0		5
[30]	$0.128 \times 0.224 \times 0.0128$	3.5, 5.5 and 6.5	2	< -15	3.49
[31]	$0.24 \times 0.32 \times 0.0128$	2.46 3.47	1.5	< -10	5 4.32
[32]	$0.34 \times 0.18 \times 0.22$	2.94–7.93	3.4	< -15	4.0–8.3
Proposed antenna	0.441×0.463	3.31 5.75 7.58	3.04–3.59 5.07–8.08	-19.4 dB -34.9 dB -21.4 dB	5.45 5.74 5.83

quency, the antenna demonstrates approximately smooth and stable polarization patterns. As the resonance frequency increases to 5.75 GHz, co-pol pattern lobes are a bit boarder, and x-pol patterns remain within limits. At 7.58 GHz, consistent directional features are observed. Finally, the CCR antenna exhibits stable patterns over all frequencies, confirming the best performance across a wide frequency range. The results show that the CCRA structure attains a good balance among gain, directivity, and radiation stability over the overall extended frequency range.

At lower bands, the surface current radiates across most of the radiating patch and ground plane, demonstrating that a major part of the structure supports in radiation is discussed in Figure 16. When the frequency becomes higher, the current accumulates mostly near the slots and edges of the conductive patch. This characteristic indicates that these regions are responsible for attaining resonance. Finally, the antenna supports better gain across all bands, proving that it is supportive for wireless applications.

The CCR antenna's gain and radiation efficiency over the frequency are explained in Figure 13. The gain remains stable, showing that the antenna delivers good performance across the band. The radiation efficiency plot, shown in Figure 13, which is highlighted in red, remains high with only small variation at higher frequencies. Without major losses, the antenna strongly transforms the power into radiated energy. The axial ratio is shown in Figure 14 with simulated and measured results. The considerable overlap between the two curves shows good agreement. The axial ratio lies below 3 dB over frequency range (1–10 GHz), indicating that the antenna achieves circular polarization with reduced losses. Finally, both results confirm the CCR antenna's reliable performance and good radiation characteristic over the desired frequency band. Figure 15 explains the 3D gain characteristics along with schematic of the patch simulated in HFSS. Table 2 explains the literature study of previous published works compared with proposed CCRA design results.

4. CONCLUSION

This study presents a compact cycle-shaped antenna capable of wideband and multiband operation. By combining concentric circular rings, spoke-like extensions, and a hexagonal slot in the ground plane, the design achieved strong resonances across two frequency ranges: 3.04–3.59 GHz and 5.07–8.08 GHz. The simple structure makes the antenna compact and low cost, and also supports tuning through geometric adjustments such as ring size, spoke length, slot dimensions, and feed position. These spokes function as additional radiating arms and alter the way currents circulate on the patch. They are particularly powerful for high frequencies (5–8 GHz) and can be tuned by their length and shape to adjust the coupling strength and bandwidth. The results confirm that the antenna maintains good impedance matching and stable performance at key frequencies of 3.31, 5.75, and 7.58 GHz, with its ability to cover sub-6 GHz, WLAN, WiMAX, and mid-band 5G applications.

REFERENCES

[1] Ansere, J. A., G. Han, L. Liu, Y. Peng, and M. Kamal, "Optimal resource allocation in energy-efficient Internet-of-Things networks with imperfect CSI," *IEEE Internet of Things Journal*, Vol. 7, No. 6, 5401–5411, 2020.

[2] Prashanth, K., B. Umamaheswari, G. Akhil, and G. V. krishna, "A compact antenna with WiMAX and WLAN bands notched for UWB applications," *International Journal of Engineering & Technology*, Vol. 7, No. 2, 489–493, 2018.

[3] Chandan, "Truncated ground plane multiband monopole antenna for WLAN and WiMAX applications," *IETE Journal of Research*, Vol. 68, No. 4, 2416–2421, 2022.

[4] Altaf, A. and M. Seo, "Dual-band circularly polarized dielectric resonator antenna for WLAN and WiMAX applications," *Sensors*, Vol. 20, No. 4, 1137, 2020.

[5] Ali, W. A. E., M. I. Ashraf, and M. A. Salamin, "A dual-mode double-sided 4 × 4 MIMO slot antenna with distinct isolation for WLAN/WiMAX applications," *Microsystem Technologies*, Vol. 27, No. 3, 967–983, 2021.

[6] Mobashsher, A. T., K. S. Bialkowski, and A. M. Abbosh, "Design of compact cross-fed three-dimensional slot-loaded antenna and its application in wideband head imaging system," *IEEE Antennas and Wireless Propagation Letters*, Vol. 15, 1856–1860, 2016.

[7] Salleh, A., C. C. Yang, M. S. J. Singh, and M. T. Islam, "Development of antipodal vivaldi antenna for microwave brain stroke imaging system," *International Journal of Engineering and Technology*, Vol. 8, No. 3, 162–168, 2019.

[8] Zebiri, C., D. Sayad, I. Elfergani, A. Iqbal, W. F. A. Mshwat, J. Kosha, J. Rodriguez, and R. Abd-Alhameed, "A compact semi-circular and arc-shaped slot antenna for heterogeneous RF front-ends," *Electronics*, Vol. 8, No. 10, 1123, 2019.

[9] Jha, P., S. Singh, and R. L. Yadava, "Wideband sub-6 GHz micro-strip antenna: Design and fabrication," in *Advances in Smart Communication and Imaging Systems*, Vol. 721, 109–115, Lecture Notes in Electrical Engineering, Springer, Singapore, 2021.

[10] Nasimuddin, *Microstrip Antennas*, InTechOpen, London, U.K., 2011.

[11] Nasimuddin, Z. N. Chen, and X. Qing, "Slotted microstrip antennas for circular polarization with compact size," *IEEE Antennas and Propagation Magazine*, Vol. 55, No. 2, 124–137, 2013.

[12] Nasimuddin, X. Qing, and Z. N. Chen, "Compact circularly polarized symmetric-slit microstrip antennas," *IEEE Antennas and Propagation Magazine*, Vol. 53, No. 4, 63–75, 2011.

[13] Nasimuddin, Z. N. Chen, and X. Qing, "Asymmetric-circular shaped slotted microstrip antennas for circular polarization and RFID applications," *IEEE Transactions on Antennas and Propagation*, Vol. 58, No. 12, 3821–3828, 2010.

[14] Shanmuganantham, T. and S. Raghavan, "Design of a compact broadband microstrip patch antenna with probe feeding for wireless applications," *AEU — International Journal of Electronics and Communications*, Vol. 63, No. 8, 653–659, 2009.

[15] Nasimuddin and Z. N. Chen, "Aperture-coupled asymmetrical C-shaped slot microstrip antenna for circular polarisation," *IET Microwaves, Antennas & Propagation*, Vol. 3, No. 3, 372–378, 2009.

[16] Reddy, V. V. and N. V. S. N. Sarma, "Compact circularly polarized asymmetrical fractal boundary microstrip antenna for wireless applications," *IEEE Antennas and Wireless Propagation Letters*, Vol. 13, 118–121, 2014.

[17] Li, J., J. Guo, A. Zhang, W. Joines, and Q. H. Liu, "Miniaturized single-feed cross-aperture coupled circularly polarized microstrip patch antenna," *Progress In Electromagnetics Research C*, Vol. 63, 183–191, 2016.

[18] Geng, L., G.-M. Wang, C.-X. Zhang, X.-J. Gao, and B.-F. Zong, "Compact circularly polarized patch antenna using a composite right/left-handed transmission line unit-cell," *Radioengineering*, Vol. 22, No. 1, 286–290, 2013.

[19] Meena, M. L. and A. Gupta, "Design analysis of a semi-circular floral shaped directional UWB antenna integrated with wireless multiband applications," *Progress In Electromagnetics Research C*, Vol. 90, 155–167, 2019.

[20] Islam, M. T., M. Cho, M. Samsuzzaman, and S. Kibria, "Compact antenna for small satellite applications [Antenna Applications Corner]," *IEEE Antennas and Propagation Magazine*, Vol. 57, No. 2, 30–36, 2015.

[21] Saha, T. K., C. Goodbody, T. Karacolak, and P. K. Sekhar, "A compact monopole antenna for ultra-wideband applications," *Microwave and Optical Technology Letters*, Vol. 61, No. 1, 182–186, 2019.

[22] Kaushal, D., T. Shanmuganantham, and K. Sajith, "Dual band characteristics in a microstrip rectangular patch antenna using novel slotting technique," in *2017 International Conference on Intelligent Computing, Instrumentation and Control Technologies (ICICICT)*, 957–960, Kerala, India, 2017.

[23] Al-Dulaimi, Z., T. A. Elwi, and D. C. Atilla, "Design of a meander line monopole antenna array based Hilbert-shaped reject band structure for MIMO applications," *IETE Journal of Research*, Vol. 68, No. 4, 2353–2362, 2022.

[24] Elwi, T. A., "Remotely controlled reconfigurable antenna for modern 5G networks applications," *Microwave and Optical Technology Letters*, Vol. 63, No. 8, 2018–2023, 2021.

[25] Gautam, A. K., A. Bisht, and B. K. Kanaujia, "A wideband antenna with defected ground plane for WLAN/WiMAX applications," *AEU — International Journal of Electronics and Communications*, Vol. 70, No. 3, 354–358, 2016.

[26] Elwi, T. A., Z. A. A. Hassain, and O. A. Tawfeeq, "Hilbert metamaterial printed antenna based on organic substrates for energy harvesting," *IET Microwaves, Antennas & Propagation*, Vol. 13, No. 12, 2185–2192, 2019.

[27] Krishnan, T., S. Sennan, V. Ravi, and D. H. reddy, "A dual-band circular patch antenna using hexagon-shaped slots," *International Journal of Communication Systems*, Vol. 35, No. 9, e5125, 2022.

[28] Erdem, H. E. and V. C. Gungor, "Analyzing lifetime of energy harvesting underwater wireless sensor nodes," *International Journal of Communication Systems*, Vol. 33, No. 3, e4214, 2020.

[29] Al Naiemy, Y., T. A. Elwi, and L. Nagy, "An end fire printed monopole antenna based on electromagnetic band gap structure," *Automatika*, Vol. 61, No. 3, 482–495, 2020.

[30] Basir, S., U. U. R. Qureshi, F. Subhan, M. A. Khan, S. A. H. Mohsan, Y. Y. Ghadi, K. Ouahada, H. Hamam, and F. Noor, "A novel monopole ultra-wide-band multiple-input multiple-output antenna with triple-notched characteristics for enhanced wireless communication and portable systems," *Sensors*, Vol. 23, No. 15, 6985, 2023.

[31] Lin, C.-K., D.-B. Lin, H.-C. Lin, and C.-C. Lin, "Design of a compact multiband monopole antenna with MIMO mutual coupling reduction," *Sensors*, Vol. 24, No. 17, 5495, 2024.

[32] Lu, P., Z. Liu, E. Lei, K. Huang, and C. Song, "Superdirective wideband array of circular monopoles with loaded patches for wireless communications," *Sensors*, Vol. 23, No. 18, 7851, 2023.